Applied Catalysis B: Environmental 218 (2017) 581–590

Contents lists available at ScienceDirect

Applied Catalysis B: Environmental

journal homepage: www.elsevier.com/locate/apcatb

Research Paper

Regenerative trapping: How Pd improves the durability of Pt diesel oxidation catalysts

Cristihan Carrillo[a], Andrew DeLaRiva[a], Haifeng Xiong[a], Eric J. Peterson[a], Michael N. Spilde[b], Deepak Kunwar[a], Ronald S. Goeke[c], Michelle Wiebenga[d], Se H. Oh[d], Gongshin Qi[d], Sivakumar R. Challa[a], Abhaya K. Datye[a,*]

[a] Department of Chemical and Biological Engineering and Center for Microengineered Materials, University of New Mexico, Albuquerque, NM 87131, USA
[b] Department of Earth and Planetary Sciences, University of New Mexico, Albuquerque, NM 87131, USA
[c] Sandia National Laboratories, Albuquerque, NM 87185, USA
[d] General Motors Global Research and Development, Chemical and Materials Systems Lab, Warren, MI 48090, USA

ARTICLE INFO

Article history:
Received 3 March 2017
Received in revised form 22 June 2017
Accepted 28 June 2017
Available online 29 June 2017

Keywords:
Catalyst sintering
Pt-Pd
Diesel oxidation catalysts
Accelerated aging
Ostwald ripening

ABSTRACT

Pt is an active component in diesel oxidation catalysts (DOCs) but it ripens to form large particles at elevated temperatures due to significant vapor phase transport of PtO_2. Adding Pd improves the durability of the catalyst but there is no clear consensus in the literature for the responsible mechanism. In this study, we examined the role of PtO_2 vapor pressure on sintering. The vapor pressure of PtO_2 was determined by measuring the emission of Pt using planar model catalysts and electron probe microanalysis (EPMA). Significant emission of Pt to the vapor phase was observed in a Pt/SiO_2 model catalyst that was aged in flowing air at 800 °C. Adding Pd lowered the rate of emission, and so did decreasing the oxygen concentration. Lowering of the vapor pressure of PtO_2 led to a decreased rate of sintering. However, the most significant decrease in sintering rate was observed in the presence of excess PdO. The excess PdO serves to trap mobile Pt species, resulting in significantly smaller Pt-Pd particles after aging in air at 800 °C for 10 h. When PtO_2 is emitted from a metallic Pt-Pd particle it can result in the formation of a separate PdO phase. Hence, in these catalysts the PdO is regenerated in the course of catalyst sintering. We propose that regenerative trapping of mobile Pt species by PdO plays an important role in improving the durability of Pt-Pd bimetallic catalysts.

1. Introduction

The USDRIVE Low Temperature Oxidation Catalyst Test Protocol recommends an accelerated aging procedure at 800 °C for diesel oxidation catalysts (DOC) [1]. However, at elevated temperatures (e.g., 800 °C), Pt sinters readily to form large particles. Adding Pd improves the durability of the catalyst but the mechanism by which this occurs is not well understood [2]. At 800 °C in the presence of oxygen Pt forms volatile PtO_2 [3] with significant vapor pressure, which is responsible for its vapor phase ripening [4,5]. Whereas under the same conditions, Pd forms a thermodynamically stable oxide of PdO with a low vapor pressure [6,7]. Morlang et al. reported an EXAFS study of $Pt-Pd/Al_2O_3$ catalysts and determined that Pd exists in both oxide and metallic form when heated under oxidizing conditions [8]. The authors proposed two possible scenarios for the location of PdO in a bimetallic catalyst; the first is that a shell of PdO surrounds the Pt-Pd particles which could block mobile Pt species from being emitted, and the second is that the PdO is present as an isolated phase. However, an HRTEM study of Pt-Pd catalysts aged in air did not find a surface layer of PdO on the Pt-Pd particles [9,10]. It is also known that the NO oxidation activity measured over Pt-Pd catalysts does not support a core-shell model [2]. This is because Pt-Pd catalysts show NO oxidation activity per Pt site that is comparable to metallic Pt despite the fact that PdO is not active for NO oxidation. Therefore, the PdO is not likely to be present on the catalyst surface in a core-shell configuration, blocking the active sites, but rather as a separate phase.

The presence of Pd in the Pt-Pd alloys would cause a lowering of the vapor pressure of PtO_2 when heated in air, as shown by Darby and Myles [11]. The extent of vapor pressure lowering would depend on the composition of the Pt-Pd alloy in the aged DOC catalyst. Chen and Schmidt showed that the Pt-Pd system should exist as a combination of the FCC metallic phase and PdO [12]. From their data, it would appear that at 750 °C in air one should expect bipha-

* Corresponding Author.
E-mail address: datye@unm.edu (A.K. Datye).

http://dx.doi.org/10.1016/j.apcatb.2017.06.085
0926-3373/

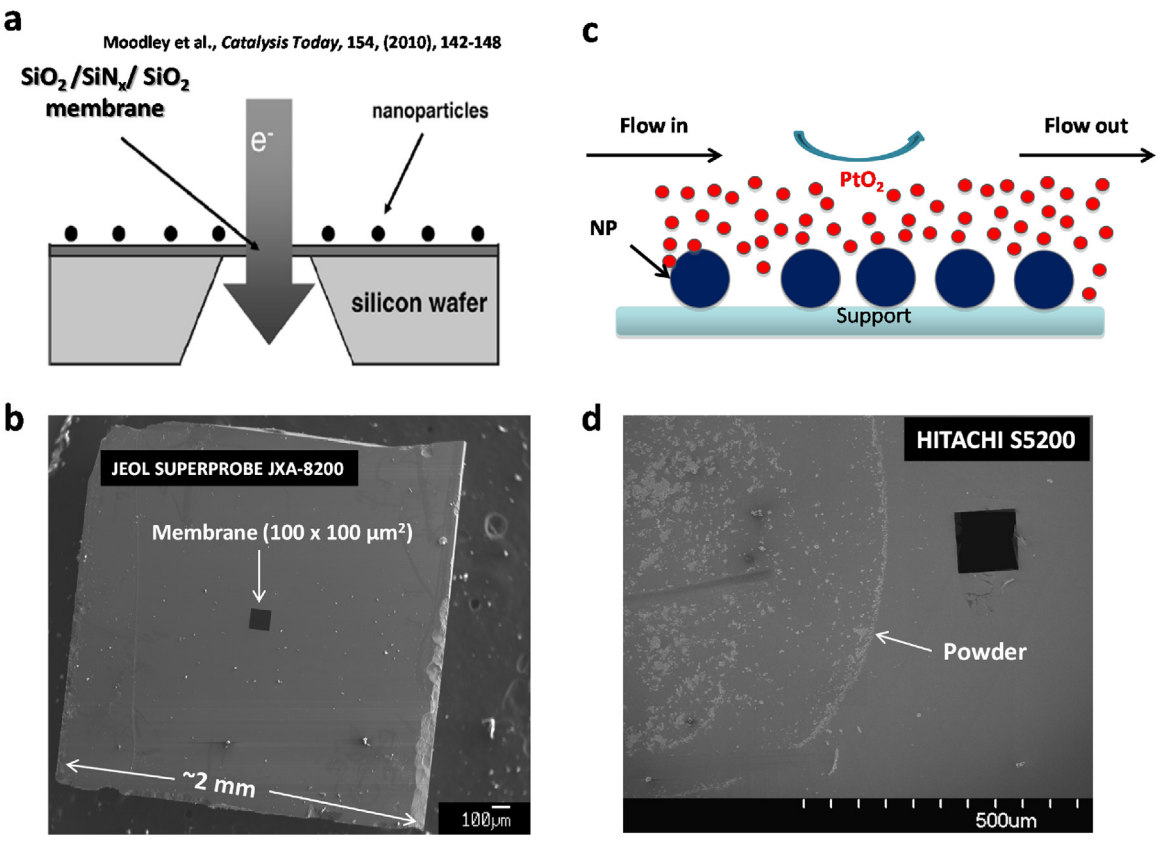

Fig. 1. (a) Side view schematic of the silicon model TEM grid taken from reference [15] (b) Low magnification SEM image with JEOL Superprobe JXA-8200 showing the top view of the model TEM grid with the $100 \times 100\,\mu m^2$ $SiO_2/SiN_x/SiO_2$ electron transparent membrane located at the center (c) Schematic of the method to evaporate and sweep away metal from the model TEM grids in order to measure emission rates (d) Hitachi S5200 SEM image showing the powder catalyst deposited on a blank model TEM grid. This was the method used in EPMA to quantify weight loadings for Pt/La-Al_2O_3 and Pt-Pd/La-Al_2O_3 powder catalysts.

sic particles. But in our previous work [4,10] we observed metallic Pt-Pd particles over a broad range of compositions, with very few biphasic particles. Since DOC aging is done at 800 °C in air, it is important to establish the composition of the FCC Pt-Pd metallic phase that is in equilibrium with PdO in this study. This will help determine the extent of lowering of the vapor pressure caused by Pd. Therefore, one of the goals in the present study is to determine the upper limit of Pd content that maintains Pt-Pd nanoparticles in metallic form under oxidizing conditions.

Another mechanism involved in enhancing the durability of Pt catalysts is atom trapping. Very simply, aging a physical mixture of Pt catalysts with either ceria [13] or with PdO [14] causes the PtO_2 species to be trapped by the oxides, which in turn leads to a decrease in Pt sintering rate. This was clearly demonstrated in a model catalyst where generation of Pt nanoparticles in the proximity of PdO caused alloying and formation of metallic Pt-Pd particles upon heating in air at 650 °C for 2 min [14]. In a previous study, it was also demonstrated that the presence of Pd lowered the emission of PtO_2 to the vapor phase [4]. Clearly the atom trapping mechanism as well as the lowering of the vapor pressure of Pt could both contribute to the enhanced durability of Pt-Pd catalysts. A systematic study is needed to determine the relative contributions of these two processes.

In this work we have examined independently the effect of both mechanisms: lowering of the PtO_2 vapor pressure and trapping of mobile Pt species. Model catalysts were used to measure the rates of PtO_2 emission. By varying the O_2 pressure we can decrease the rate of emission of PtO_2 from a Pt-only model catalyst until it becomes equal to that from a Pt-Pd model catalyst. Having established similar vapor pressures, those conditions were used to age powder catalysts at 800 °C. Over a broad range of compositions, only metallic Pt-Pd nanoparticles were found in the aged samples. By adding excess Pd to the catalyst, a separate PdO phase was introduced which helps to trap mobile Pt. The catalysts that contain excess PdO exhibit the smallest Pt-Pd particle sizes showing the importance of regenerative trapping in this catalyst system.

2. Experimental

2.1. Catalyst preparation & aging

2.1.1. Pt and Pt-Pd model catalysts

The model catalysts used in this study were silicon wafer model TEM grids ($4\,mm^2$) which were developed by Moodley et al. at Eindhoven University of Technology [15]. Samples contain a $100 \times 100\,\mu m^2$ electron transparent membrane film at the center that is 15 nm thick. The membrane film is composed of SiO_2/SiN_x which forms ~3 nm surface oxide at the top and bottom of the film upon heating in air. A side view schematic and SEM image showing the top of the model TEM grids may be seen in Fig. 1a and b. Pt and Pd metals were deposited directly onto the surface of the model TEM grids using 10 kV Temescal electron beam evaporator equipped with a high vacuum cryo-pumped system. The system was pumped to a base pressure of 1×10^{-7} Torr prior to depositions. The equivalent metal film thicknesses were controlled by a quartz crystal microbalance (QCM) and the deposition rates were controlled to 0.03 Å/s. A continuous film was not formed during deposition because these transition metals are non-wetting on oxide surfaces at very low loadings. Hereafter the Pt and Pt-Pd metals supported on the SiO_2/SiN_x will be referred to as "Pt/SiO_2" and

"Pt-Pd/SiO_2" respectively for simplicity.The nominal loading of Pt in the Pt/SiO_2 sample was 500 pm (picometer) equivalent film thickness. The total nominal loading of metal in the Pt-Pd/SiO_2 sample was also 500 pm (250 pm Pt + 250 pm Pd). These loadings amount to an initial atomic ratio of 1Pt:1Pd in the bimetallic Pt-Pd SiO_2 sample.

The model catalysts were pretreated prior to metal emission experiments in order to allow the deposited films to de-wet and form nanoparticles. The pretreatments were also performed in order to stabilize nanoparticle sintering and to begin with the same initial particle size/fractional surface area between Pt and Pt-Pd. The pretreatments were performed by placing the samples in an open boat and heating in a tube furnace. Pt/SiO_2 samples were pretreated in flowing air (100 sccm) at 650 °C for 30 min whereas Pt-Pd/SiO_2 samples were pretreated in flowing 7% H_2 (100 sccm) at 700 °C for 20 min. The H_2 pretreatment was needed to increase the mean particle size to make it comparable to that of Pt/SiO_2.

Metal emission studies were performed at 800 °C under flowing gas at 100 sccm. The same tube furnace and open boat geometry were used as described above for the pretreatment procedure. Since the vapor pressure of PtO_2 is very high at 800 °C (1.6×10^{-3} Pa), the sweeping of volatilized Pt was achieved by flowing gas over the sample during aging (Fig. 1c). This was the method used by Alcock and Hooper to determine the nature of the Pt volatile oxide [3]. Therefore, it was very important to keep the gas flow rate constant during every aging experiment since the extent of Pt emission depends on the rate of "sweeping". The furnace was ramped up to and stabilized at 800 °C prior to inserting a sample and thermocouple in order to age for precise times. The sample was immediately taken out after aging for the desired time and characterized with electron probe microanalysis (EPMA) and transmission electron microscopy (TEM).

2.1.2. La-Al_2O_3 supported Pt, Pd, and Pt-Pd powder catalysts

Monometallic 1.6 wt% Pt/La-Al_2O_3 and 5.6 wt% Pd/La-Al_2O_3 catalysts were synthesized via incipient wetness technique. The monometallic Pt catalyst was synthesized with a chloroplatinic acid (H_2PtCl_6) precursor that was introduced to a lanthanum-stabilized alumina (La-Al_2O_3) powder after having been diluted with de-ionized water. The monometallic Pd catalyst was made in the same manner using a $Pd(NO_3)_2$ precursor. The slurries were dried overnight and calcined at 550 °C for 2 h. Bimetallic Pt-Pd/La-Al_2O_3 catalysts with varying Pt:Pd compositions were synthesized in order to study the effect of Pd on the durability of Pt-Pd particles. The compositions ranged from Pt-rich to Pd-rich in order to study samples that contain metallic particles vs. those that contain metallic particles + oxide (excess PdO). A 1.3 wt% Pt-Pd/La-Al_2O_3 (1.1 wt% Pt/0.2 wt% Pd) catalyst (Pt-rich) was synthesized first with $Pd(NO_3)_2$ and H_2PtCl_6 precursors and was prepared in the same manner as the monometallic catalysts. The initial atomic ratio in this catalyst corresponds to 1Pt:0.33Pd. Catalysts with varying Pd concentrations were then synthesized by adding additional $Pd(NO_3)_2$ precursor to the initial bimetallic batch (1Pt:0.33Pd). All powder samples were calcined at 550 °C for 2 h. In this series of catalysts, the amount of Pt is kept constant (1.1 wt%) while the amount of Pd is changed to go from 1Pt:0.33Pd (Pt-rich) to 1Pt:9Pd (Pd-rich). Weight loadings were determined with EPMA in which powders were deposited onto blank model TEM grids. The catalysts were first crushed in a mortar and pestle and dispersed in ethanol. A drop of the solution was then placed on a blank model TEM grid which allowed for characterization of the powder in EPMA. An image of the resultant powder deposit is shown in Fig. 1d. A summary of the Pt-Pd catalysts investigated in this study is presented in Table 1.

The powder catalysts were aged in the same tube furnace and open boat geometry used for the model catalysts. The boat was loaded with 200 mg of the catalyst and the aging was performed at 800 °C for 10 h with flowing gas fed at 100 sccm. 1.6 wt% Pt/La-Al_2O_3 catalysts were aged at various oxygen concentrations ranging from 0 to 21% O_2. Note that 0% O_2 concentration corresponds to aging in N_2 and 21% O_2 corresponds to aging in air. The O_2 concentrations were varied by mixing air with nitrogen while holding the total flow rate constant at 100 sccm. 5.6 wt% Pd/La-Al_2O_3 and Pt-Pd/La-Al_2O_3 catalysts were aged in flowing air. Particle sizes were characterized after aging with X-ray Diffraction (XRD) and TEM.

Table 1
Summary of Pt-Pd/La-Al_2O_3 powder catalysts with various Pt:Pd atomic ratios.

Sample Name	Atomic Ratio Pt:Pd	Pt-Pd Total Loading (wt%)	Overall Pd At%
1Pt:0.33Pd	1:0.33	1.3	25
1Pt:1Pd	1:1	1.5	50
1Pt:1.5Pd	1:1.5	1.7	60
1Pt:3Pd	1:3	2.5	75
1Pt:6Pd	1:6	5.1	85
1Pt:9Pd	1:9	6.8	90

2.2. Catalyst characterization

2.2.1. Transmission electron microscopy

Transmission electron microscopy (TEM) was performed at 200 kV using a JEOL 2010 FEG (Field Emission Gun) TEM/STEM equipped with an Oxford energy dispersive X-ray spectroscopy (EDS) detector. Particles were counted using high-angle annular dark field (HAADF) scanning transmission electron microscopy (STEM) images. HAADF-STEM was performed using a 0.5 nm probe under high resolution mode. The volume average diameter, d_v was determined by the relation $d_v = \frac{\sum n_i d_i^4}{\sum n_i d_i^3}$ Inter-planar spacings of Pt-Pd nanoparticles in the model catalysts were measured under high-resolution TEM (HRTEM) mode. The composition of Pt-Pd nanoparticles in the model catalysts was studied with single-particle EDS using a 1 nm probe diameter in the analysis mode in the HAADF-STEM. All TEM images and EDS data were analyzed using Digital Micrograph and Oxford INCA software.

2.2.2. Electron probe microanalysis

Metal concentrations were quantified with an electron probe microanalyzer (EPMA). EPMA was performed using wavelength dispersive X-ray spectroscopy (WDS) with a JEOL JXA-8200 Super-Probe operated at 10 kV with a 10 μm probe diameter and 30 nA probe current. The change in metal concentrations after aging model catalysts was determined by calculating the equivalent film thickness using GMRFilm software [16]. Based on thin film calculations performed with the GMRFilm, metal films under ~75 Å were deposited with electron beam evaporation so as to remain in the region in which the X-ray intensities (K-ratios) scale linearly with film thickness. The thin film setup used in the GMRFilm calculations is described in the supplemental information (SI) along with the definition of K-ratios and standards used for elemental analysis (Fig. S1). K-ratios were obtained over several regions of the sample where the average K-ratio found in the experiment was used to determine the equivalent metal film thickness. See Fig. S1 in the SI for the equations relating film thickness to K-ratios. The standards used for elemental analysis of the La-Al_2O_3 supported Pt, Pd, and Pt-Pd powder catalysts are shown in Table 1 of the SI.

2.2.3. X-ray diffraction

X-ray diffraction patterns for aged Pt/La-Al_2O_3, Pd/La-Al_2O_3, and Pt-Pd/La-Al_2O_3 powder catalysts were obtained with a Rigaku Smart Lab system equipped with a D/teX X-ray detector. The Cu anode and a Ni filter were operated at 40 kv and 40 mA and the samples were irradiated over the 2θ range of 5–150 in steps of 0.02°. The crystallite sizes were estimated with Jade software by

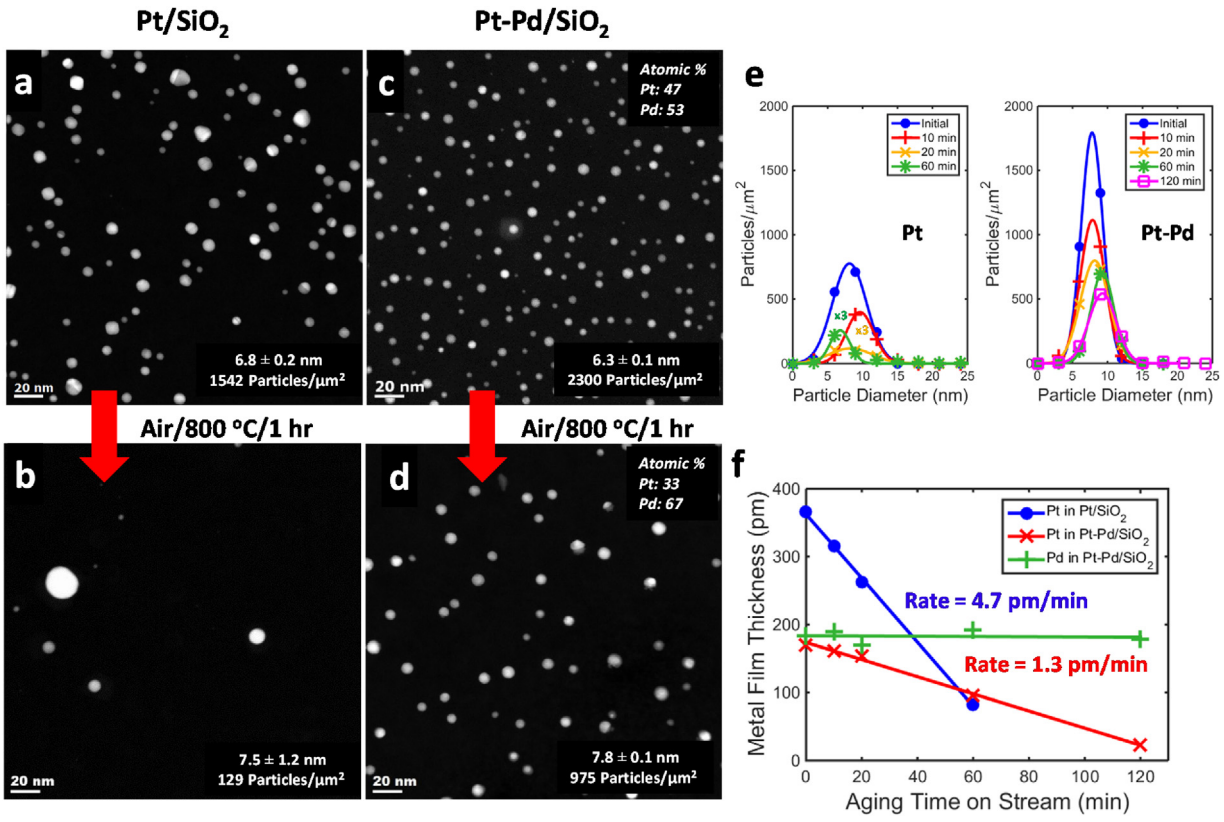

Fig. 2. Aging of Pt/SiO_2 and $Pt\text{-}Pd/SiO_2$ model catalyst in flowing air (100 sccm) at 800 °C (a) HAADF-STEM image of the initial state of Pt/SiO_2 (b) HAADF-STEM image after aging Pt/SiO_2 for 1 h (c) HAADF-STEM image of the initial state of $Pt\text{-}Pd/SiO_2$ (d) HAADF-STEM image after aging $Pt\text{-}Pd/SiO_2$ for 1 h (e) Evolution of the Pt/SiO_2 and $Pt\text{-}Pd/SiO_2$ particle size distribution during aging. Note the Pt PSD was multiplied by a factor of 3 for 20 min and 60 min aging in order to see the PSD more clearly (f) Equivalent metal film thickness vs aging time on stream as determined by EPMA.

applying the Williamson-Hall method [17] and Scherrer equation, $\tau = \frac{K\lambda}{\beta cos\theta}$ with $K = 0.9$ and $\lambda = 1.5406$ Å. The diffraction peaks were fitted with a Pseudo-Voigt function.

2.3. Reactivity measurements

2.3.1. CO oxidation

CO oxidation activity of the aged $Pt/La\text{-}Al_2O_3$ catalyst was measured in a U-tube stainless steel reactor which was heated in a high temperature oven. Light-off curves were obtained at a ramp rate of 2 °C/min from 25 to 300 °C. The gas composition was 1.9 vol% CO and 1.3 vol% O_2 balanced by He at a gas hourly space velocity (GHSV) of 77,500 h^{-1}. The gases were injected every 3 min and analyzed with a Varian CP-4900 Micro Gas Chromatograph.

3. Results

3.1. Metal emission from model catalysts

The monometallic Pt/SiO_2 sample was prepared by depositing Pt onto model TEM grids via electron beam evaporation. EPMA analysis on the sample after deposition showed that the initial Pt film thickness was 366 pm. Following depositions, the samples were pretreated in flowing air (100 sccm) in a tube furnace at 650 °C for 30 min. Note, that the "initial" sample refers to the state after the pretreatment (Fig. 2a). The emission of Pt was studied in flowing air (100 sccm) at 800 °C after aging for desired lengths of time. The number of Pt particles dropped significantly (1542 → 129 particles/μm^2) after aging for just 1 h in flowing air at 800 °C (Fig. 2a, b, and e). HAADF-STEM images of Pt/SiO_2 after each aging duration may be referenced in Fig. S2a–d of the SI. Note that the shape and peak position of the Pt particle size distribution (PSD) in Fig. 2e did not change significantly during aging (mean particle sizes remains between 5 and 10 nm). This indicates that Ostwald ripening (and associated Pt particle growth) was not involved to a significant degree, but rather the sweeping of volatilized Pt by the flowing air caused a loss of Pt from the sample and a drop in the number of Pt particles. As will be shown below, however, the vapor phase mediated ripening of Pt is significant in powder catalysts in the presence of O_2 at 800 °C, which leads to the formation of large particles. Formation of large particles was not observed in the model catalyst since it is an open system and any volatilized metal is swept away by the flowing air rather than contributing to ripening.

The role of Pd on the emission of Pt was studied by preparing $Pt\text{-}Pd/SiO_2$ model catalysts in a similar manner via electron beam evaporation. The initial catalyst contained a nominal 1Pt:1Pd atomic ratio which was co-deposited. The actual amounts deposited correspond to 170 pm of Pt and 184 pm of Pd. Therefore, the $Pt\text{-}Pd/SiO_2$ catalyst contained about half of the Pt that was present on the monometallic Pt/SiO_2 sample. Both samples had comparable initial amounts of total metal (~360 pm). The $Pt\text{-}Pd/SiO_2$ model catalyst was pretreated in flowing 7% H_2 (100 sccm) at 700 °C for 20 min (Fig. 2c) and this resulted in an initial particle size of 6.3 ± 0.1 nm that was comparable to that of the monometallic Pt particles of 6.8 ± 0.2 nm (Fig. 2a). Metal emission measurements from the bimetallic $Pt\text{-}Pd/SiO_2$ sample were performed at 800 °C in the same manner as the monometallic Pt/SiO_2 sample. Clearly, fewer Pt-Pd particles disappeared (2300 → 975 particles/μm^2) after aging in flowing air at 800 °C for 1 h (Fig. 2c, d, and e). Notice that the disappearance of particles is accompanied by some degree of particle growth, consistent with Ostwald ripen-

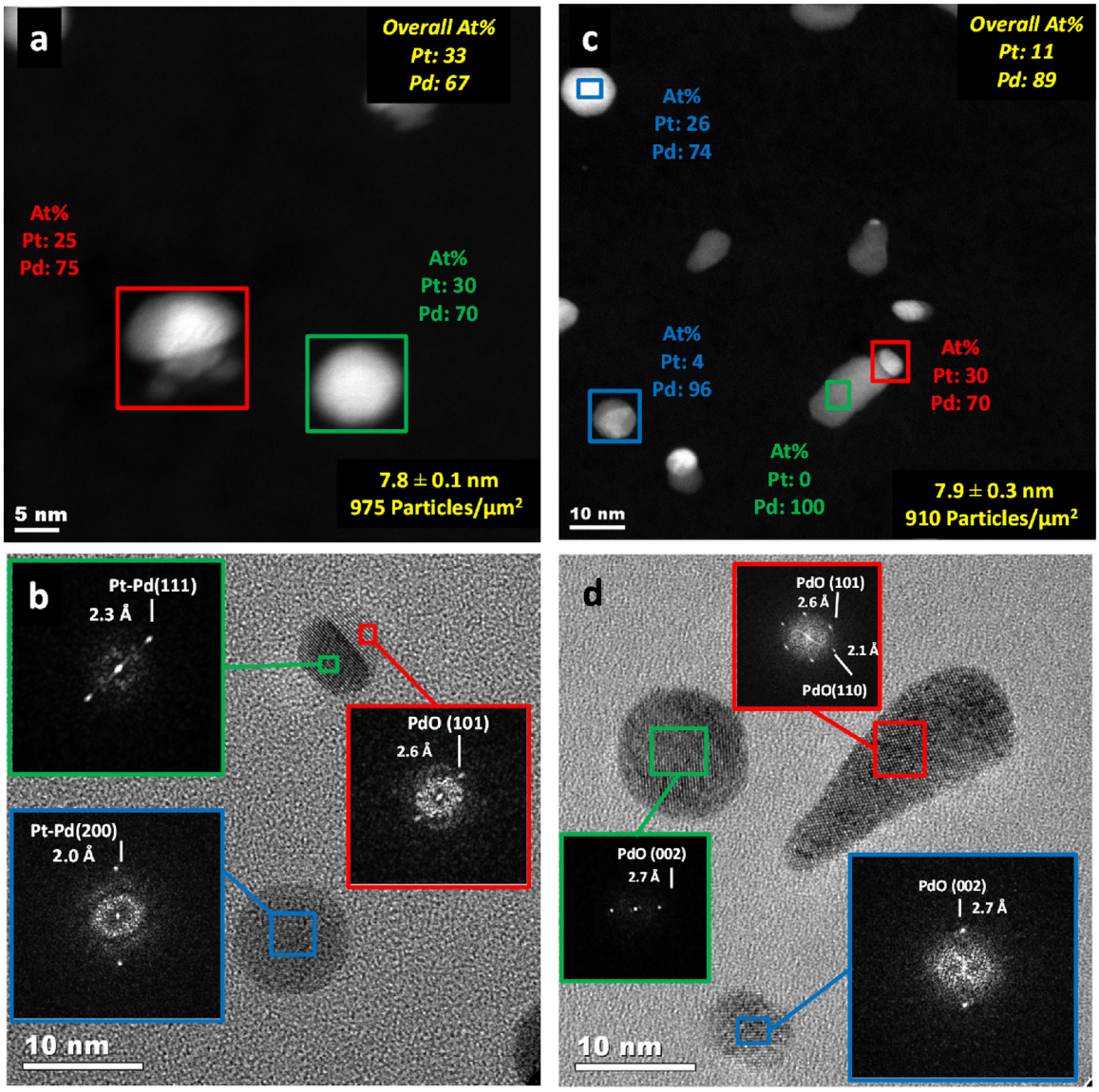

Fig. 3. Microstructure evolution of the Pt-Pd/SiO_2 model catalyst during aging in flowing air (100 sccm) at 800 °C (a) HAADF-STEM image of Pt-Pd/SiO_2 model catalyst after aging for 1 h. Color coded boxes and text show which particles were analyzed in single-particle EDS along with Pt and Pd concentrations (b) HRTEM image of Pt-Pd/SiO_2 model catalyst after aging for 1 h. Insets are color coded fast fourier transforms (FFTs) for corresponding particles showing the lattice plane orientation and spacings (c) HAADF-STEM image of Pt-Pd/SiO_2 model catalyst after aging for 2 h. Color coded boxes and text show which particles were analyzed in single-particle EDS along with Pt and Pd concentrations (d) HRTEM image of Pt-Pd/SiO_2 model catalyst after aging for 2 h. FFT insets are color coded with each particle showing the lattice plane orientation and spacings.

ing, as evidenced by the PSD shown in Fig. 2e. See Fig. S2e-i of the SI for HAADF-STEM images of Pt-Pd/SiO_2 after each aging duration.

The equivalent metal film thicknesses for Pt/SiO_2 and Pt-Pd/SiO_2 samples were measured with EPMA after aging for several durations in flowing air at 800 °C (Fig. 2f). As was observed in the Pt PSD (Fig. 2e), significant Pt was lost to the vapor phase and swept away, giving rise to the decrease in Pt film thickness (Fig. 2f). If the rate of Pt emission was proportional to the remaining amount of Pt, one would expect a first-order process leading to an exponential dependence on time. Instead, it was found that the Pt emission followed a zero-order process with a constant emission rate of 4.7 pm/min. We postulate that a boundary layer of volatile PtO_2 is at equilibrium with the metal and hence, the emission rate depends only on the vapor pressure of PtO_2. A similar approach was used in the work of Alcock and Hooper [3] who pointed out that as long as the flow rate of gas was low, the rate of Pt emission was directly proportional to the flow rate and the concentration of Pt in the vapor phase (which is related to its vapor pressure). Our experimental conditions with a low flow rate of gas which was kept constant in all the experiments, resemble those of Alcock and Hooper [3]. Adding Pd lowered the emission of Pt by 72% in the Pt-Pd sample during aging (Fig. 2f). No loss of Pd was observed, however, because the vapor pressure of PdO (2×10^{-7} Pa in air at 1 atm) is four orders of magnitude lower than that of PtO_2 (1.6×10^{-3} Pa in air at 1 atm) [3,6,7]. However, some ripening of the Pt-Pd particles caused an overall increase in average Pt-Pd particle size (Fig. 2c, d, and e), as was also observed in our previous study [4]. It is interesting to note that the extent of Pt emission reduction in the Pt-Pd/SiO_2 sample was greater than expected based on the assumption of an ideal solution of Pt and Pd in the alloy. One would expect the emission of Pt to be decreased by 50% given the initial 1Pt:1Pd atomic ratio in the Pt-Pd/SiO_2 catalyst. Results of single-particle EDS and HRTEM presented in the next section help rationalize this observation.

3.1.1. Aging-Induced changes in microstructure of Pt-Pd/SiO_2 model catalysts

As Pt was lost, Pt-Pd particles became rich in Pd (Fig. 3a) and caused the formation of biphasic particles that were detected in the sample after aging for 1 h (Fig. 3b). Therefore, the microstructure of Pt-Pd nanoparticles in the model catalyst was studied with single-particle EDS and HRTEM to understand the changes in morphology/composition during aging and how they may affect the emission of Pt. Single-particle EDS after 1 h of aging (Fig. 3a) showed that Pt-Pd particles contained about 25–30 at% Pt which compared well with the overall atomic ratio determined in EPMA. Lattice spacing analysis via HRTEM after aging for 1 h revealed that PdO grew forming a coherent interface with Pt-Pd (Fig. 3b). PdO (101) grew epitaxially with Pt-Pd (111) as previously seen by Kan and Weaver [18] with Pd (111). See Fig. S3 and Fig. S4 in the SI for more images of PdO (101) growing epitaxially with Pt-Pd (111) and more single-particle EDS. The individual particle compositions were different from the overall sample composition after aging for 2 h due to the existence of a pure PdO phase in addition to Pt-Pd (Fig. 3c). Some spherical particles contained around 25–30 at% Pt while others contained only Pd and the particles seemed to taper with a metallic core at the end of the tail. We suspect as Pt is lost and the PdO phase segregates, the particle will shrink in size and move on the surface causing the appearance of a tail. The particles that tapered left behind PdO with a lower contrast than the tip/core that contained ~25–30 at% Pt (Fig. 3c). HRTEM analysis after aging for 2 h revealed the tails were PdO with 2.6 and 2.1 Å lattice spacings corresponding to the PdO (101) and PdO (110) planes, respectively (Fig. 3d). More HRTEM analysis after aging for 2 h may be seen in Fig. S4 of the SI. The observations suggest that a coherent interface between Pt-Pd (111) and PdO (101) is possible but is only seen when there is a well-defined Pt-Pd (111) surface facet. The 25–30 at% Pt in the core of nanoparticles is in line with the earlier observation that Pt emission was lowered by ~72% in the bimetallic Pt-Pd/SiO_2 sample compared to the Pt/SiO_2 sample. Furthermore, single-particle EDS and HRTEM showed no evidence of a PdO shell surrounding the bimetallic Pt-Pd nanoparticles as previously shown by Gremminger et al. [19]. Therefore, we conclude that the lowering of Pt emission is caused primarily by the formation of a Pt-Pd alloy and our results suggest that the upper limit of Pd concentration that is stable in the Pt-Pd metallic phase at 800 °C in air is ~70%, which is consistent with the phase diagram proposed by Chen and Schmidt [12].

3.1.2. Effect of O_2 concentration on the emission of Pt in the Pt/SiO_2 model catalyst

The effect of oxygen concentration (0–21% O_2) on the emission of Pt from the monometallic Pt/SiO_2 model catalyst was studied during aging at 800 °C for 1 h. Our results in Fig. 4 show that decreasing the O_2 concentration lowered Pt emission rates. The emission rate of PtO_2 from the Pt/SiO_2 sample aged in 5.5% O_2 was comparable to the rate at which PtO_2 was lost from the bimetallic Pt-Pd/SiO_2 sample aged in air (21% O_2).

3.1.3. Effect of O_2 concentration on the sintering of the Pt/La-Al_2O_3 powder catalyst

The effect of vapor pressure on the sintering of Pt in a 1.6 wt% Pt/La-Al_2O_3 catalyst was studied by varying the O_2 concentration from ~0% O_2 (99.99% N_2) to 21% O_2 (air). The "initial" sample in Fig. 5a refers to the catalyst after calcination at 550 °C for 2 h. No peak was observed in the Pt (111) region due to sub-nanometer sized Pt particles as can be seen in Fig. 5a. The XRD peaks in the aged samples got sharper with increasing O_2 concentration at 800 °C for 10 h indicating that the Pt crystallite size increased. Crystallite size analysis with the Scherrer equation and the Williamson-Hall method implemented in the Jade software showed that the Pt crystallite size increased linearly with increasing O_2 concentration (Fig. 5b). The same linear trend and comparable particle sizes were observed with STEM where the particle size is reported as the volume average diameter (Fig. 5b). HAADF-STEM images and PSDs of the Pt catalysts are shown in Fig. S5 of the SI. Temperature programmed CO oxidation was performed on the catalysts aged under various O_2 concentrations (Fig. 5c and d). The temperature was ramped from 25 to 300 °C at a rate of 2 °C/min and the gas composition was 1.9 vol% CO and 1.3% O_2 balanced by He at a GHSV of 77,500 h^{-1}. The catalyst was clearly deactivated due to aging, with the effect being more severe with aging under higher O_2 concentrations (Fig. 5c and d). The XRD and CO oxidation activity data in Fig. 5 demonstrate that Pt sintering rates are related to the pressure of O_2. The loss of Pt from powder catalysts was also studied in the same experimental setup. More details are provided in the SI. No significant loss of Pt from the powder catalysts was detected (Table II and III of the SI) because nearly all of the Pt particles are located inside the micropores and thus the vaporized Pt would not be expected to be swept away, as observed with the model catalysts. This leads to significant sintering of metal particles (without Pt loss) in the powder catalyst.

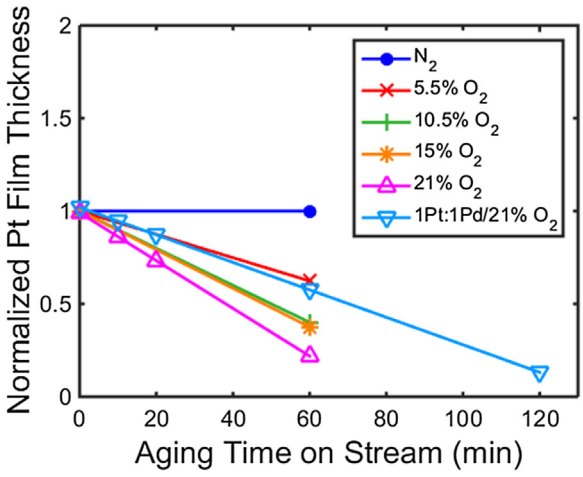

Fig. 4. Effect of O_2 concentration on the emission of Pt in Pt/SiO_2 model catalysts. Normalized Pt film thickness (final thickness/initial thickness) is plotted against aging time on stream. Aging was done in a mixture of flowing air + N_2 (100 sccm) at 800 °C.

3.1.4. Effect of Pd concentration on the sintering of Pt-Pd/La-Al_2O_3 powder catalysts

In order to investigate bimetallic powder catalysts we prepared a powder catalyst that contained a 1Pt:0.33Pd atomic ratio (1.1 wt% Pt/0.2 wt% Pd on La-Al_2O_3 support) which was calcined at 550 °C for 2 h. To study the role of Pt:Pd ratio, Pd was added via impregnation to the 1Pt:0.33Pd catalyst. Therefore, in this series of catalysts the loading of Pt was held constant at 1.1 wt% and the Pd loading was increased up to a total loading of 6.8 wt% Pt-Pd as shown in Table 1. In terms of atomic ratios the samples varied in concentration from 1Pt:0.33Pd (Pt-rich) to 1Pt:9Pd (Pd-rich). Each sample was calcined at 550 °C and aged in air at 800 °C for 10 h.

The results of XRD analysis are shown in Fig. 6a and Table 2. HAADF-STEM images and PSDs of the Pt-Pd catalysts may be seen in Fig. S6 of the SI. Aging of these catalysts caused Pt-Pd to sinter significantly as seen by the Pt-Pd (111) peaks. The XRD data shows the absence of the Pt-Pd (111) peak in the sample before aging (after calcination at 550 °C), indicating that the particle size is too small to be detected by XRD (Fig. 6a). Furthermore, the Pt-Pd (111) peak overlaps with the alumina peaks, making it difficult to detect when the size of the peak is very small. After aging (800 °C

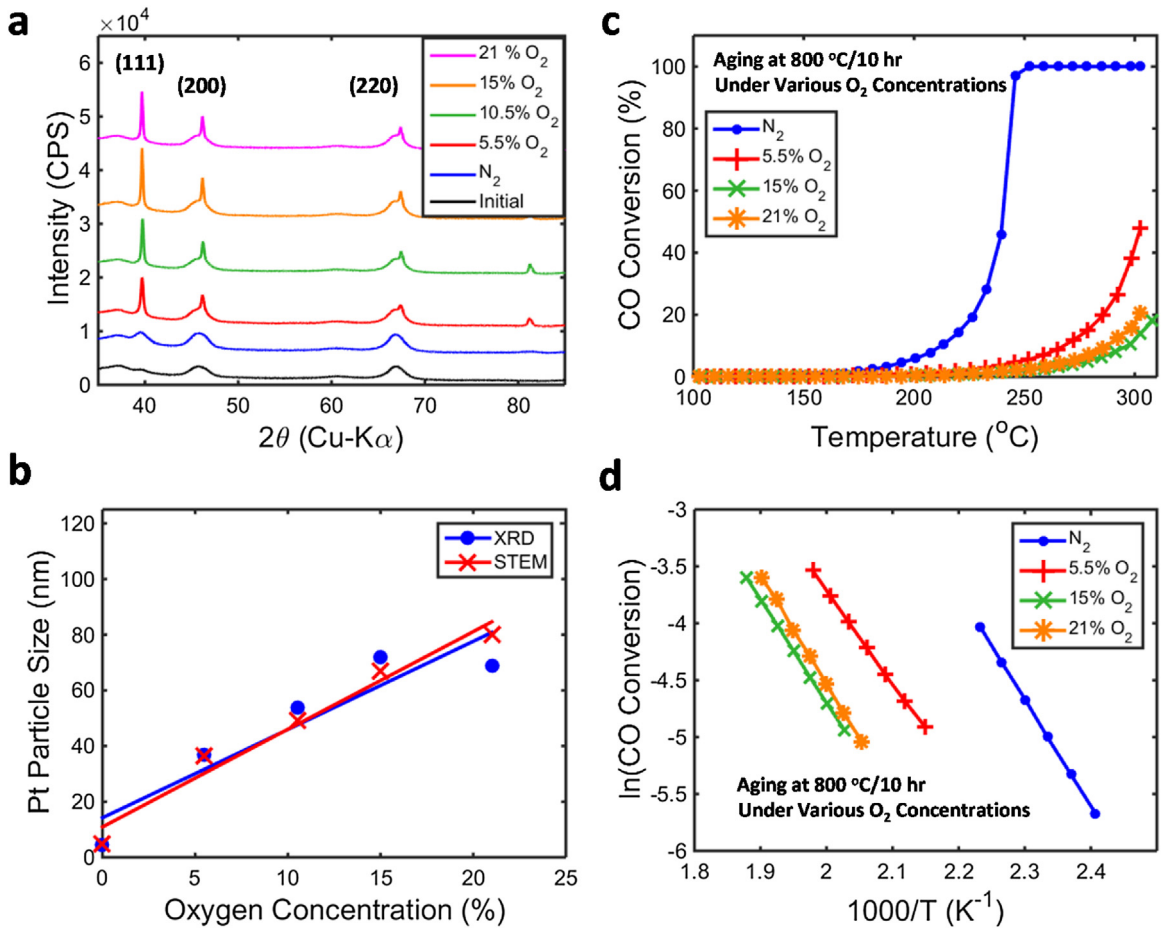

Fig. 5. Aging of 1.6 wt% Pt/La-Al_2O_3 powder catalysts under various O_2 concentrations at 800 °C for 10 h with a total gas flow rate of 100 sccm (a) XRD patterns obtained from Cu-Kα radiation after aging (b) Pt particle size vs O_2 concentration. Particle sizes were determined with XRD and volume average diameters determined from HAADF-STEM images (c) Light-off measurements for CO oxidation after aging. Temperatures were ramped at 2 °C/min from 25 to 300 °C. Note, data is only shown in the range of 100–300 °C due to no reactivity below 100 °C. Gas compositions were 1.9 vol% CO and 1.3 vol% O_2 balanced by He at a GHSV of 77,500 h^{-1} (d) Arrhenius plots determined in the range of 0.75–3% CO conversion from Fig. 5c.

Table 2
XRD summary of alumina-supported powder catalysts after aging in air at 800 °C for 10 h.

Sample	EPMA (Overall Pd At%)	Metallic Crystallite Size (nm)	Oxide Crystallite Size (nm)	Lattice Constant (Å)	Vegard's Law Estimate (Pd At%)
100% Pt	0	69	–	3.928 ± 0.002	0
1Pt:0.33Pd	25	54	–	3.910 ± 0.001	43
1Pt:1Pd	50	59	–	3.910 ± 0.002	43
1Pt:1.5Pd	60	52	–	3.906 ± 0.002	55
1Pt:3Pd	75	40	–	3.904 ± 0.002	62
Pt/5.5% O_2	0	36	–	3.928 ± 0.002	0
1Pt:6Pd	85	34	26	3.898 ± 0.001	79
1Pt:9Pd	90	18	40	3.899 ± 0.001	75
100% Pd	100	–	17	–	100

for 10 h), however, the Pt-Pd (111) peak in the 1Pt:0.33Pd sample became very sharp. As the Pd content was increased, the Pt-Pd (111) peak became broader (Fig. 6a). Zooming into the Pt-Pd (111) peak (Fig. 6b) it can be seen more clearly that the peak gets broader as more Pd is added. There was also a shift in the lattice constant indicating the formation of the Pt-Pd alloy. Table 2 shows that the composition of the metallic phase becomes Pd-rich after aging, eventually reaching a composition around 75 at% Pd as derived from Vegard's law analysis. However, the broad Pt-Pd peaks, and variation in compositions in individual particles as seen by STEM-EDS, make it difficult to derive precise compositions from the XRD analysis. The results are consistent with the TEM observations indicating an upper limit of Pd concentration in the metallic phase of about 70 at% Pd. This upper limit is consistent with the STEM and EDS data shown in Fig. 3.

It was clearly shown in the Pt-Pd/SiO_2 model catalyst that Pd lowers the vapor pressure of PtO_2 as measured by the rates of emission (Fig. 2). The lower rate of PtO_2 emission may also be achieved by reducing the O_2 pressure. To investigate the role of emission rates, the sintering of the 1.6 wt% Pt-only catalyst in 5.5% O_2 was compared with that of the 1Pt:3Pd catalyst in air. The 1Pt:3Pd catalyst is the first sample in the series to show the presence of a separate PdO phase. The composition of this catalyst is also close to the upper limit of phase stability of metallic Pt-Pd. Therefore, a comparison of these two catalysts demonstrates the role of lower-

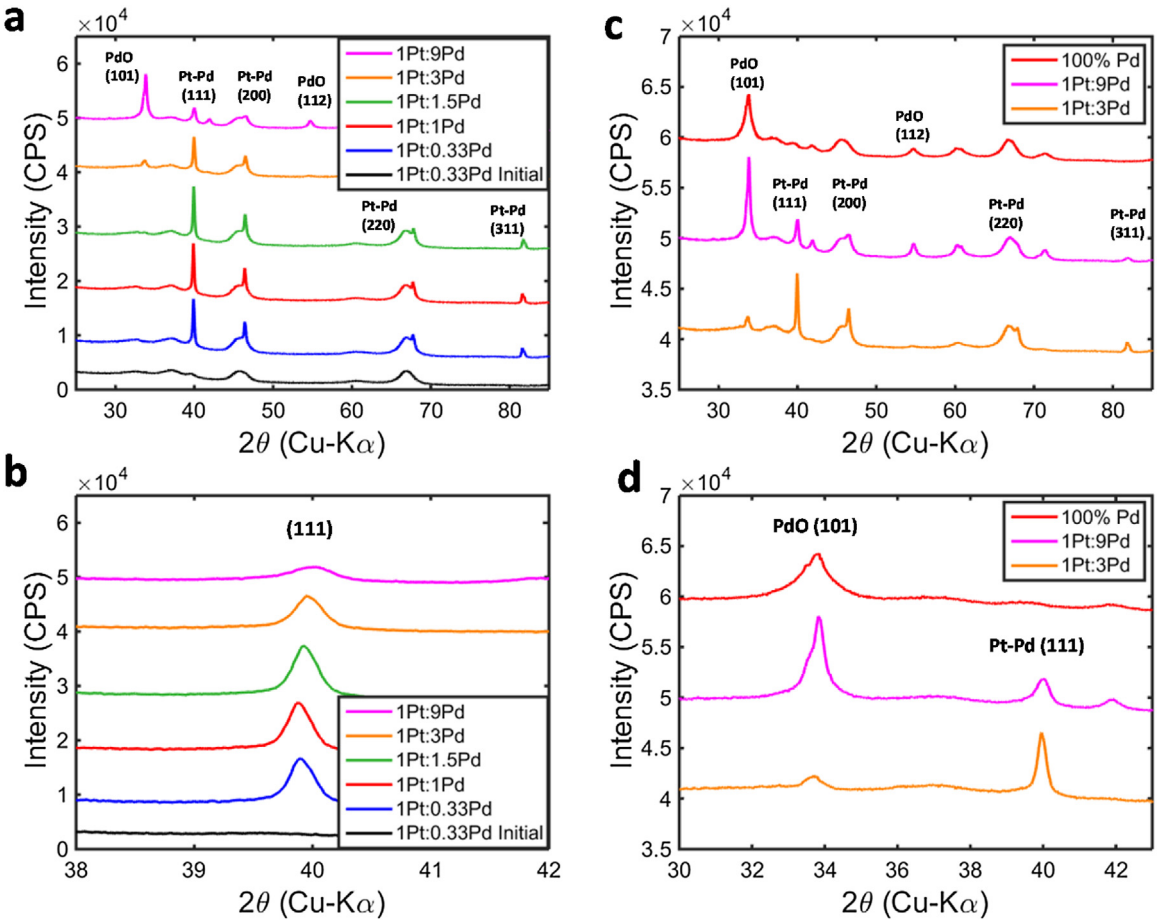

Fig. 6. XRD after aging Pt-Pd/La-Al_2O_3 powder catalysts in flowing air (100 sccm) at 800 °C for 10 h. Note, the numbers in the legends refer to Pt:Pd atomic ratios (a) XRD patterns obtained with Cu-Kα radiation (b) Zoom-in on the Pt-Pd (111) peak from (a). (c) XRD pattern comparison between a pure Pd sample and two Pd-rich Pt-Pd samples (d) Zoom-in on the PdO (101) and Pt-Pd (111) region of (c).

ing the emission of PtO_2. As seen in Table 2, the crystallite sizes are similar for these two catalysts (36 vs 40 nm).

As Pd concentration is further increased (1Pt:6Pd and 1Pt:9Pd), a limiting composition of the metallic phase was reached. Note the XRD pattern for the 1Pt:6Pd sample was placed in Fig. S7 of the SI in order to conserve space in the plots of Fig. 6. The extra Pd leads to the formation of a separate PdO phase as seen clearly in the XRD patterns (Fig. 6a and 6c). It is in this range of compositions that a further broadening of the metallic Pt-Pd (111) peak was observed. This cannot occur due to a lowering of the vapor pressure of PtO_2 since the upper limit for the stability of metallic Pt-Pd was reached. Clearly another mechanism must be responsible. It is also interesting that there is a significant effect of the Pt on the rate of sintering of the Pd phase. This is shown clearly in Fig. 6c and d, where the results of aging the Pd-only catalyst are compared with the bimetallic catalysts that have a separate PdO phase (Table 2: 40 nm in the bimetallic vs 17 nm in the Pd-only).

4. Discussion

This work has shown that emission rates of Pt can be directly measured by using model catalysts where the PtO_2 is swept away by the flowing air. The rapid equilibrium between the catalyst and the vapor phase in the boundary layer allows us to determine the rate of loss of Pt from the vapor pressure of PtO_2. Pt emission to the vapor phase is significant at 800 °C under oxidizing conditions where a majority of the Pt was lost after 1 h of aging. Adding Pd decreased the rate of emission by ~72% because the Pt-Pd alloy particles that are stable under these conditions consist of about 70 at% Pd. Virtually no Pd emission was observed due to the low vapor pressure of PdO. The vapor pressures determined by the model catalyst experiments help rationalize the sintering rates observed in the powder catalysts. When comparing a Pt-only catalyst with a Pt-Pd catalyst that has a similar vapor pressure of PtO_2, the final size of the metallic particles after aging was comparable, as evidenced by XRD data (Fig. 6 and Table 2). This indicates that the vapor pressure of the metal oxide mobile species is an important factor in determining the rate of catalyst sintering under oxidizing aging conditions considered here. This result is in agreement with the work of Plessow et al. who performed modeling of PtO_2 vapor phase transport to demonstrate the role of O_2 pressure in Pt sintering [5].

The role of Pd goes beyond lowering of the vapor pressure of PtO_2 over the Pt-Pd bimetallic particles since PdO also serves to trap the mobile Pt species. As discussed above, PdO has a vapor pressure four orders of magnitude lower than that of PtO_2 and thus very little sintering of the Pd-only catalysts is observed when heated in air at 800 °C. While PdO is thermodynamically stable, the formation of metallic Pt-Pd was observed when mobile PtO_2 species interact with the PdO [14]. Therefore, Pt causes the reduction of PdO and the resulting Pt-Pd metal particles can undergo Ostwald ripening [4]. This is why the Pd sinters much faster when Pt is also present in the same catalyst (Table 2). The PdO crystallite size in the 1Pt:9Pd sample (40 nm) was much larger than the Pd-only catalyst (17 nm). Clearly, the Pt facilitates the sintering of the PdO phase and therefore, the excess PdO is not just a spectator. Fig. 7 shows

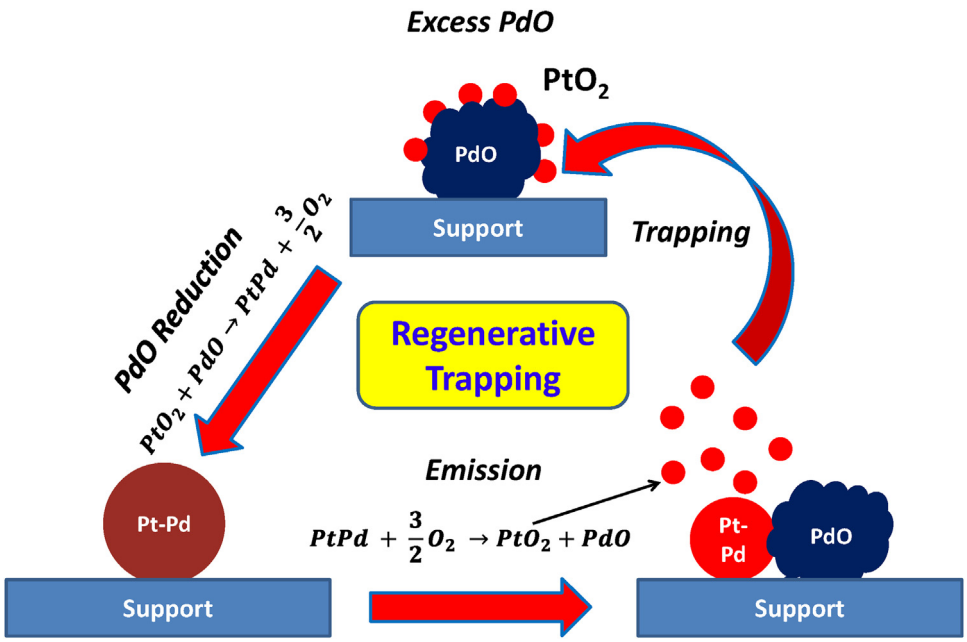

Fig. 7. Schematic showing the regenerative trapping mechanism.

a schematic of the Pt-Pd interaction. This latter process we have termed "regenerative trapping".

As shown in Fig. 7, PdO provides sites for trapping mobile PtO_2 which was confirmed experimentally on a model catalyst [14] as well as when a $Pt/MgAl_2O_4$ powder was physically mixed with PdO/Al_2O_3 and aged in air [20]. The reaction between PtO_2 and PdO causes the formation of metallic Pt-Pd in flowing air, even at temperatures as low as 650 °C [14]. One would expect that capture of mobile PtO_2 would consume all of the PdO, but when there is excess Pd beyond what is stable thermodynamically in metallic form, the balance would exist as a separate PdO phase. This PdO has been called "excess PdO" in Fig. 7. Furthermore, emission of PtO_2 from Pt-Pd would also cause the formation of PdO as shown in Fig. 3. The formation of PdO due to the emission of PtO_2 from metallic Pt-Pd therefore leads to the regenerative nature of the trapping cycle. The beneficial effect of regenerative trapping is only seen when a separate PdO phase is present in the catalyst. In our study, an excess of Pd was used to demonstrate the role of regenerative trapping and to separate this effect from the lowering of the vapor pressure. In industrial catalysts, these processes must occur regardless of the actual Pt:Pd ratio used because emission of Pt could generate PdO if the composition of the particle goes beyond the limit of phase stability.

These observations lead us to conclude that the role of Pd in a bimetallic Pt-Pd catalyst is two-fold. On one hand, Pd helps to lower the vapor pressure of Pt, thereby slowing the rates of sintering. In the presence of excess PdO a second mechanism becomes operative leading to significant slowing of the rate of Pt sintering. We suggest that regenerative trapping plays an important role in the observed durability of Pt-Pd catalysts.

5. Conclusions

The role of PtO_2 vapor pressure on bimetallic Pt-Pd catalyst sintering was investigated by aging catalysts in air at 800 °C for 10 h. Lowering the vapor pressure of PtO_2 slows down the rate of sintering. The lowering of the vapor pressure was achieved by decreasing the O_2 concentration or by alloying Pt with Pd, both of which had a similar effect on the final particle size. When a Pt-Pd particle is heated in an open system, emission of PtO_2 causes the formation of a metallic core of Pt-Pd and a separate PdO phase. The upper limit of stability of metallic Pt-Pd in air at 800 °C was determined to be about 70 at% Pd. The separate PdO phase generated during Pt emission from Pt-Pd particles plays an important role since it serves to trap mobile PtO_2 species. This leads to a mechanism which we have termed "regenerative trapping", since the PdO traps are regenerated by the emission of PtO_2 from the Pt-Pd alloy particles. While Pd by itself remains very stable during heating at 800 °C in air, Pt-Pd particles continue to sinter since mobile Pt as well as mobile Pd species can be emitted from metallic Pt-Pd particles. This work provides a fundamental understanding of the sintering mechanism of Pt-Pd catalysts which would be helpful for the future development of more durable Pt-Pd diesel oxidation catalysts.

Acknowledgements

This work is financially supported by the NSF GOALI Grant CBET-1438765 and by the Chemical and Materials Systems Lab at GM Global R&D. The authors would like to thank Sandia National Laboratories for the use of the 10 kV Temescal electron beam evaporator. Sandia National Laboratories is a multi-mission laboratory managed and operated by Sandia Corporation, a wholly owned subsidiary of Lockheed Martin Corporation, for the U.S. Department of Energy's National Nuclear Security Administration under contract DE-AC04-94AL85000.

Appendix A. Supplementary data

Supplementary data associated with this article can be found, in the online version, at http://dx.doi.org/10.1016/j.apcatb.2017.06.085.

References

[1] USDRIVE, Aftertreatment Protocols for Catalyst Characterization and Performance Evaluation: Low-Temperature Oxidation Catalyst Test Protocol, 2015.
[2] G.W. Graham, H.W. Jen, O. Ezekoye, R.J. Kudla, W. Chun, X.Q. Pan, R.W. McCabe, Catal Letters 116 (2007) 1–8.
[3] C.B. Alcock, G.W. Hooper, Proc. R. Soc. London Ser A—Math. Phys. Sci. 254 (1960) 551–561.

[4] T.R. Johns, R.S. Goeke, V. Ashbacher, P.C. Thune, J.W. Niemantsverdriet, B. Kiefer, C.H. Kim, M.P. Balogh, A.K. Datye, J. Catal. 328 (2015) 151–164.
[5] P.N. Plessow, F. Abild-Pedersen, ACS Catal. 6 (2016) 7098–7108.
[6] G. Bayer, H.G. Wiedemann, Thermochim. Acta. 11 (1975) 79–88.
[7] M. Peuckert, J. Phys. Chem. 89 (1985) 2481–2486.
[8] A. Morlang, U. Neuhausen, K.V. Klementiev, F.W. Schütze, G. Miehe, H. Fuess, E.S. Lox, Appl. Catal. B: Environ. 60 (2005) 191–199.
[9] M.R. Ward, T. Hyde, E.D. Boyes, P.L. Gai, ChemCatChem 4 (2012) 1622–1631.
[10] T.R. Johns, J.R. Gaudet, E.J. Peterson, J.T. Miller, E.A. Stach, C.H. Kim, M.P. Balogh, A.K. Datye, ChemCatChem 5 (2013) 2636–2645.
[11] J.B. Darby, K.M. Myles, Metall. Trans 3 (1972) 653–657.
[12] M. Chen, L.D. Schmidt, J. Catal. 56 (1979) 198–218.
[13] J. Jones, H. Xiong, A.T. DeLaRiva, E.J. Peterson, H. Pham, S.R. Challa, G. Qi, S. Oh, M.H. Wiebenga, X.I. Pereira Hernandez, Y. Wang, A.K. Datye, Science 353 (2016) 150–154.
[14] C. Carrillo, T.R. Johns, H. Xiong, A. DeLaRiva, S.R. Challa, R.S. Goeke, K. Artyushkova, W. Li, C.H. Kim, A.K. Datye, J. Phys. Chem. Lett. 5 (2014) 2089–2093.
[15] P. Moodley, F.J.E. Scheijen, J.W. Niemantsverdriet, P.C. Thune, Catal. Today 154 (2010) 142–148.
[16] R.A. Waldo, An Iteration Procedure to Calculate Film Compositions and Thicknesses in Electron-Probe Microanalysis, San Francisco Press, San Francisco, 1988.
[17] G.K. Williamson, W.H. Hall, Acta Metall. 1 (1953) 22–31.
[18] H.H. Kan, J.F. Weaver, Surf. Sci. 603 (2009) 2671–2682.
[19] A.T. Gremminger, H.W. Pereira De Carvalho, R. Popescu, J.D. Grunwaldt, O. Deutschmann, Catal. Today. 258 (2015) 470–480.
[20] H. Xiong, E. Peterson, G. Qi, A.K. Datye, Catal. Today. 272 (2016) 80–86.